Journal of Innovative Optical Health Sciences
Vol. 11, No. 4 (2018) 1850015 (11 pages)

DOI: 10.1142/S1793545818500153

Synthetic aperture-based linear-array photoacoustic tomography considering the aperture orientation effect

Xiangwei Lin*,‡, Jaesok Yu†, Naizhang Feng*,¶ and Mingjian Sun*,§
*Department of Control Science and Engineering
Harbin Institute of Technology, Harbin
Heilongjiang 150001, P. R. China
†Department of Bioengineering, University of Pittsburgh
Pittsburgh, PA 15213, USA
‡lin_xiangwei@yeah.net
§sunmingjian@hit.edu.cn
¶fengnz@yeah.net

Received 28 December 2017
Accepted 25 February 2018
Published 21 March 2018

The synthetic aperture-based linear-array photoacoustic tomography (PAT) was proposed to address the limited-view shortcomings of the single aperture, but the detection field of view (FOV) determined by the aperture orientation effect was not fully considered yet, leading to the limited-view observation and image resolution degradation. Herein, the aperture orientation effect was proposed from the theoretical model and then it was verified via both the numerical simulation and phantom experiment. Different orientations were enumerated sequentially in the simulation to approximate the ideal full-view case for the optimal detection FOV, considering the detection pattern of the linear-array transducer. As a result, the corresponding optimal aperture orientation was 60° if the synthetic aperture was seamlessly established by three single linear arrays, where the overlapped detection pattern was optimized from the individual linear-array transducer at the adjacent positions. Therefore, the limited-view artifacts were minimized and the image resolution was enhanced in this aperture orientation. This study showed that the aperture orientation had great influence on the optimal detection FOV in the synthetic aperture configuration, where the full-view imaging quality and enhanced image resolution could be achieved.

Keywords: Photoacoustic tomography; synthetic aperture; aperture orientation; linear-array transducer.

§,¶Corresponding authors.

1. Introduction

Photoacoustic tomography (PAT) is a promising biomedical imaging modality which is based on the thermoacoustic effect in biological tissues.[1–3] It combines the superiorities of high contrast of optical imaging and high spatial resolution of ultrasound imaging. The linear-array PAT is widely applied because it has high-speed data acquisition, handheld convenience, and unique capability of detecting optical absorbers up to several centimeters in depth.[4–8] The linear-array-based single aperture PAT suffers from the limited-view challenge due to its incomplete detection geometry,[9–11] thus the synthetic aperture PAT was proposed to address the problem. However, the optimal detection field of view (FOV) mainly determined by the aperture orientation cannot always be full view in practice, considering the target structure, acoustic coupling, and laser irradiation pattern. For example, the human breast is hemispherical in shape and cannot be immersed in water entirely for acoustic coupling. Therefore, it is of great significance to study the aperture orientation effect in the synthetic aperture PAT.

Several synthetic aperture PATs have been proposed with different aperture orientations. Huang *et al.* utilized acoustic reflector to increase the detection angle of single aperture, and the geometry was either one reflector placed at 45° (Ref. 12) or two reflectors located at 120° to triple the detection view.[13] Cox and co-workers also chose the acoustic reflectors and a novel reverberant cavity to enhance the view of single aperture.[14,15] However, the detection FOV is limited if the acoustic reflectors is placed in the detection area and the corresponding acoustic properties need to be carefully assigned. Kruger *et al.* and Yang *et al.* focused on the relative rotation between the transducer and imaging targets to increase the detection coverage, rotating either the imaging targets[16] or the linear-array transducer.[17] Lin *et al.* applied an extended linear-array transducer to form the synthetic aperture.[18] Nonetheless, the aperture orientation effect in these methods was not fully considered yet, resulting in obvious limited-view artifacts, resolution degradation, and huge dataset to achieve the full-view observation with the linear-array transducer.[19] Therefore, the orientation of the acoustic reflector, reverberant cavity, and the relative rotation angle should be carefully taken into account to find the optimal detection field of view, where the full-view imaging quality and enhanced image resolution could be achieved with the reduced measurement.

In this work, the aperture orientation effect in the synthetic aperture PAT was studied, which had originated from the rectangular detection pattern of the linear array and the photoacoustic (PA) imaging reconstruction theory. Then this effect was verified through both the numerical simulation and phantom experiment. The most commonly used reconstruction algorithm in photoacoustic imaging is the universal back-projection method.[20–23] It assumes an enclosed detection surface, but this ideal full-view condition cannot always be satisfied in the single linear-array-based synthetic aperture PAT, considering the rectangular detection pattern and photon penetration depth.[24–26] Therefore, the optimal aperture orientation was enumerated based on the numerical model, where a series of orientations were set to find the optimal one that could produce the preferable detection FOV. On the condition of optimal aperture orientation, the corresponding phantom experiment was conducted to verify the above findings. In addition, the three-dimensional photoacoustic imaging ability in this optimal aperture orientation was also demonstrated in the synthetic aperture PAT.

2. Methods

2.1. *Theoretical model in the synthetic aperture PAT reconstruction*

The PA effect leads to the generation of acoustic waves through the absorption of nanosecond-width short-pulsed laser energy. On the condition of thermal and stress confinements, part of the absorbed energy would be converted into heat, generating the wideband PA signal due to the transient thermoelastic expansion.[27–29] Via the propagation in the biological tissue, the PA signal would then be detected at the tissue boundary by the transducer, either a single element or an array ultrasound transducer. The mathematical model for presenting the forward problem for an acoustically homogeneous medium is

$$p_d(r_d, t) = \frac{1}{4\pi c}\frac{\partial}{\partial t}\int dA \frac{p_0(r)}{|r_d - r|}\bigg|_{ct=|r_d-r|}. \quad (1)$$

Its physical meaning is that the pressure p_d at the spatial point r_d and time t is proportional to the time derivative of the integral of the absorbed laser energy over a circle centered at r_d with radius ct in two-dimensional case. The most common inverse reconstruction model to restore the photoacoustic image is

$$p_0(r) = \frac{1}{4\pi c^2} \times \int dS \frac{1}{t}\left[\frac{p_d(r_d,t)}{t} - \frac{\partial p_d(r_d,t)}{\partial t}\right]\Bigg|_{ct=|r_d-r|}. \quad (2)$$

From the theoretical model of forward PA signal propagation and backward PA image reconstruction, the ideal tomographic imaging configuration assumes that the imaging objects are fully surrounded by detectors on a closed surface. Nonetheless, in the synthetic aperture PAT, the generated PA signals from the absorbers in the overlapped region would be detected at only parts of the omni-directional propagation due to the aperture orientation effect. The visible structures are perpendicular to each surface of the individual aperture, and the imaging targets cannot always be accessed from all directions and are fully enclosed by the detectors, resulting in the loss of structure information. In addition, the aperture size of the probe and the penetrated depth of the photoacoustic signals are finite and restricted,[9] leading to the limited-view artifacts and image resolution degradation in the conventional rectangular detection area of the single linear-array PAT. Thus the aperture orientation is a key factor and it should be carefully assigned in the synthetic aperture PAT.

The illustration of the aperture orientation effect in the linear-array-transducer-based synthetic aperture PAT is shown in Fig. 1. The optimal detection FOV of the linear-array transducer is commonly rectangular (the green dashed line) to avoid the grating lobes, where its width is the same as array's width and the depth is determined by the elevational focus properties of the transducer.[30–32] Moreover, the analytic explanation of the limited-view problem related to the detector aperture geometry has already been studied,[10] putting forward the concept of the visible detection regions (the blue shaded area). In the synthetic aperture PAT, the multi-view configuration determined by the

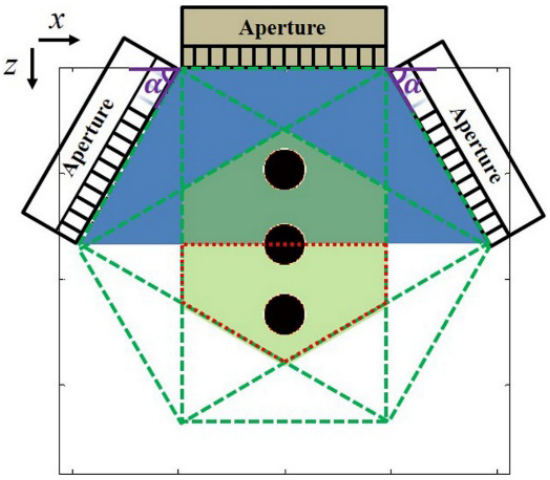

Fig. 1. Schematic of aperture orientation effect in the synthetic aperture PAT.

aperture orientation α would produce an overlapped detection region (the green shaded area). The targets in the visible detection regions could be free from the limited-view problem. However, the targets located outside the blue shaded region but still in green shaded area, especially the area surrounded by the red dotted line, still suffer from the limited-view problem or do not need further investigation.

2.2. *Numerical model of the aperture orientation effect*

To approximate the enclosed detection trajectory with the synthetic aperture, numerical simulation was carried out first to find the optimal aperture orientation α and validate its feasibility. A k-Wave MATLAB toolbox was chosen for the forward PA wave propagation[33] and the corresponding PA images were restored via the universal back-projection reconstruction method. Two tilted arrays of the three individual linear ones were placed at different angles α to form the synthetic aperture configuration. The conceptual simulation models of the optimal detection FOV in the nearly full-view observation and enhanced resolution are separately shown in Fig. 2. The single aperture settings are depicted in Figs. 2(a) and 2(c), while the synthetic aperture configurations are illustrated in Figs. 2(b) and 2(d), respectively.

The flat single apertures with 128 and 128×3 elements were assigned for comparison, while the

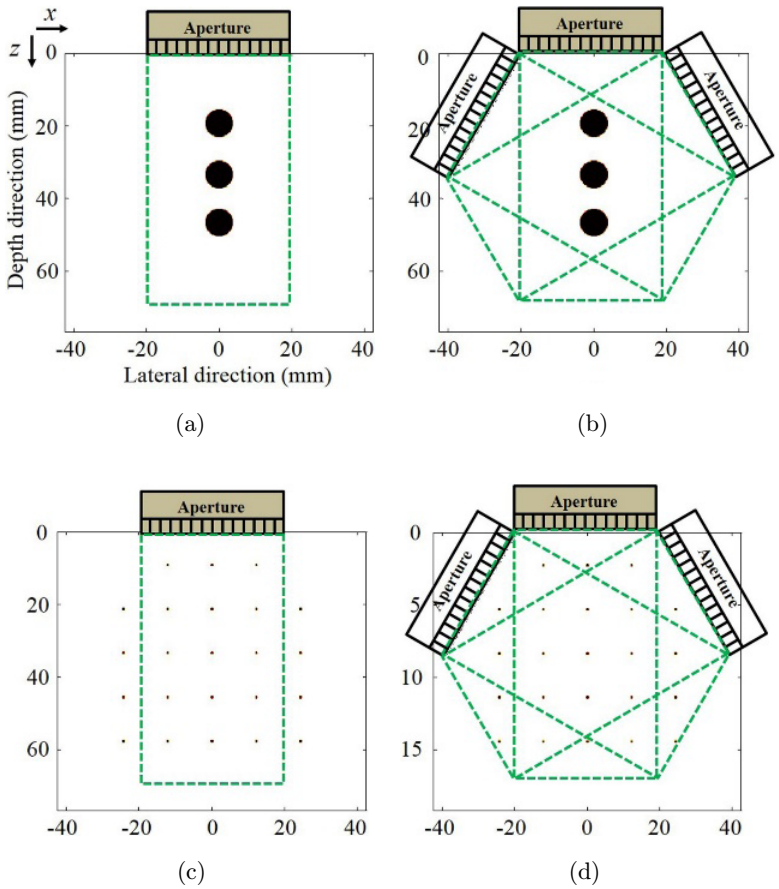

Fig. 2. Numerical model of aperture orientation effect in synthetic aperture PAT. Limited-view problem demonstrated respectively in (a) single aperture and (b) synthetic aperture. Enhanced resolution model shown in (c) single aperture and (d) synthetic aperture, respectively.

synthetic aperture was formed by the multi-view extended linear array with different aperture orientations α. The synthetic aperture was composed of three individual linear-array transducers, and it had 128×3 elements in total, each of the linear array consisting of 128 directional elements with the pitch of 0.30 mm and 5.0 MHz center frequency. These transducer parameters were the same with those of ATL L7-4 transducer used in the following experiment. The properties and locations of the acoustic sources in the medium were defined as spatially smoothed initial pressure distribution, assuming that the laser uniformly illuminated the target. The distribution of the targets in the limited-view reconstruction was three numerical disks located in different regions, whereas the point targets in the enhanced resolution model were uniformly distributed in much wider regions. These areas were respectively belonging to the visible detection region, overlapped detection region, and the other areas in addition to above regions (as shown in Fig. 1).

2.3. *PA experiment setup for the phantom study*

The feasibility of the proposed assumption was subsequently verified through the phantom study. The corresponding synthetic aperture with 60° aperture orientation was calibrated first, and then the phantom study was conducted by relatively rotating the imaging phantom to match the synthetic aperture setup in the simulation, as shown in Fig. 3. The synthetic aperture PA experiment setup was initiated once the tunable pump laser-based (Vibrant HE532I, OpoTek, CA, USA) optical parametric oscillator (OPO) emits a 5-ns-width laser pulse at 700 nm, where the laser pulse repetition rate is 10 Hz. The output light was delivered by the custom-made full-ring optical fiber to ensure

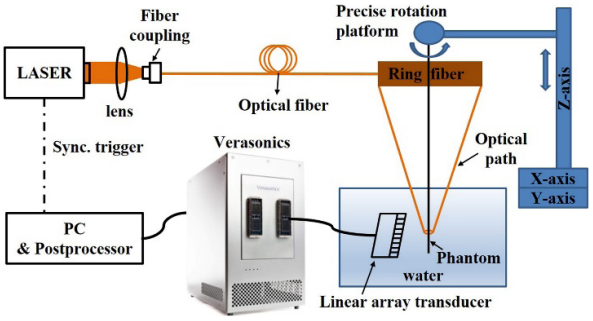

Fig. 3. The experiment setup of synthetic aperture PAT.

that the light uniformly illuminated the target. The external trigger signal from the laser system was sent to synthesize the receive-only mode on Verasonics photoacoustic imaging platform. The generated PA signal would be captured by ATL L7-4 linear-array transducer, and then reconstructed by the back-projection algorithm in a personal computer (PC) with post-processor.

3. Results

3.1. *Limited-view simulation of aperture orientation effect*

Figures 4(a)–4(f) are the PA images of a series of numerical disks, where the targets are located in different detection regions. Figures 4(a) and 4(b) show the results from the flat single aperture, with 128 elements and 128×3 elements, respectively. From these two reference images, the single aperture PAT obviously has the limited-view defects, still existing in a larger aperture. Thus different tilted aperture orientations were designed to form the synthetic aperture setup, as shown in Fig. 2(b). Considering the target geometry, aperture width, detection pattern, and photon penetration depth, the tilted orientations α in the synthetic aperture are enumerated as 45°, 60°, 75°, and 90°, respectively. These increasing orientations are assigned to find the optimal angle to approximate the full-view reconstruction theory in the synthetic aperture PAT, where the tradeoff between the limited-view problem and the adequate detection FOV is achieved.

Figures 4(c)–4(f) are the corresponding PA images restored from the related aperture orientations. Comparing single aperture recovered PA images with others, the synthetic aperture PAT can really improve the image quality and visualize the target structure more completely. In the synthetic aperture recovered PA images with different aperture orientations, the shape of recovered disks in the first row is similar, whereas Fig. 4(d) demonstrates

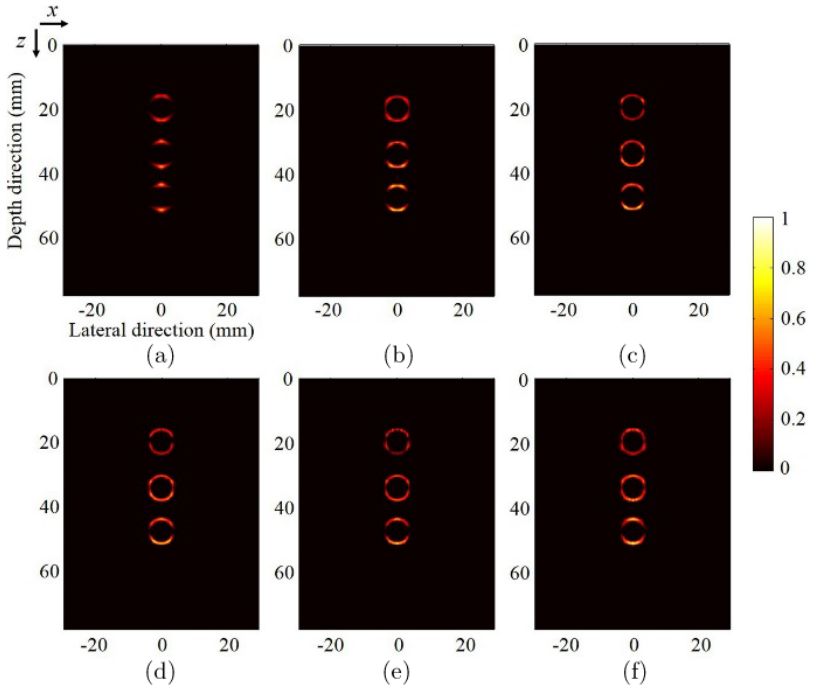

Fig. 4. Numerical simulation results of limited-view problem in synthetic aperture PAT. PA images recovered from single aperture with (a) 128 and (b) 128×3 elements. (c)–(f) PA images recovered from aperture orientations of 45°, 60°, 75°, and 90°, respectively.

a bit more structure information for the second disk and much complete structure information for the third disk than its counterparts. This happens because the aperture orientation of 60° matched with the enclosed detection trajectory in the theoretical model. As the aperture orientation increases, more complete target structure in depth direction could be observed with a limited imaging depth, such as the third disk in Fig. 4(f) that has already been located outside the visible detection regions (the blue shaded area in Fig. 1). The detection FOV at 45° is inappropriate due to elevational focus in the real transducer. Moreover, the detection FOV at 60° in the lateral direction is larger than the cases of 75° and 90°, as the lateral detection FOV is decreased with increase of the orientation.

3.2. *Enhanced resolution simulation of the optimal aperture orientation*

To verify that the optimal detection FOV is really achieved when the aperture orientation is 60°, the point spread function is measured through a series of point targets, which are distributed uniformly in the whole area of individual rectangular detection pattern of the three linear-array transducers, as shown in Fig. 2(d). The corresponding reconstructed PA images shown in Figs. 5(a) and 5(b) are the results from the single aperture configuration, while Figs. 5(c)–5(f) are recovered from the synthetic aperture with the aperture orientations of 45°, 60°, 75°, and 90°, respectively. It could be easily discerned that the image resolution from the synthetic aperture is obviously improved. However, as the aperture orientation increased, the synthetic aperture configuration could cover less target structure in depth and also the target in the lateral direction could be missed. For example, the point targets in the boundary cannot be detected at 90°, as shown in Fig. 5(f). Also, the shape of the point target becomes blurred if its location is too close to the transducer [as indicated by the arrows in Fig. 5(e)]. Moreover, the target shape is similar in the whole region, and the overall imaging contrast is much uniform in the synthetic aperture configuration.

Figure 6 shows the normalized lateral intensity profiles in PA images [see Figs. 5(c)–5(f)], which

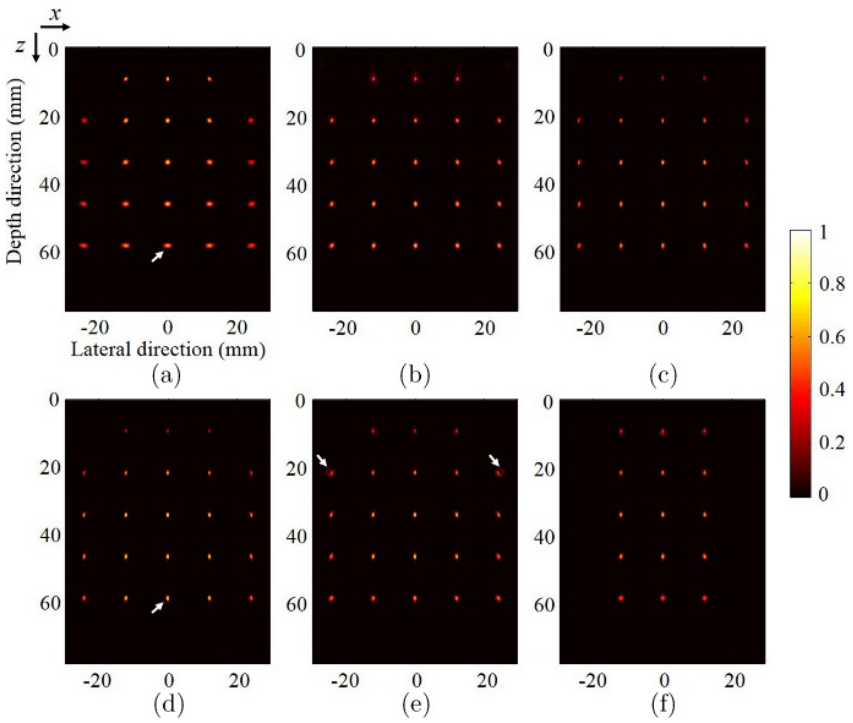

Fig. 5. Numerical simulation results of enhanced resolution in synthetic aperture PAT. PA images recovered from single aperture with (a) 128 and (b) 128×3 elements. (c)–(f) PA images recovered from aperture orientations of 45°, 60°, 75°, and 90°, respectively.

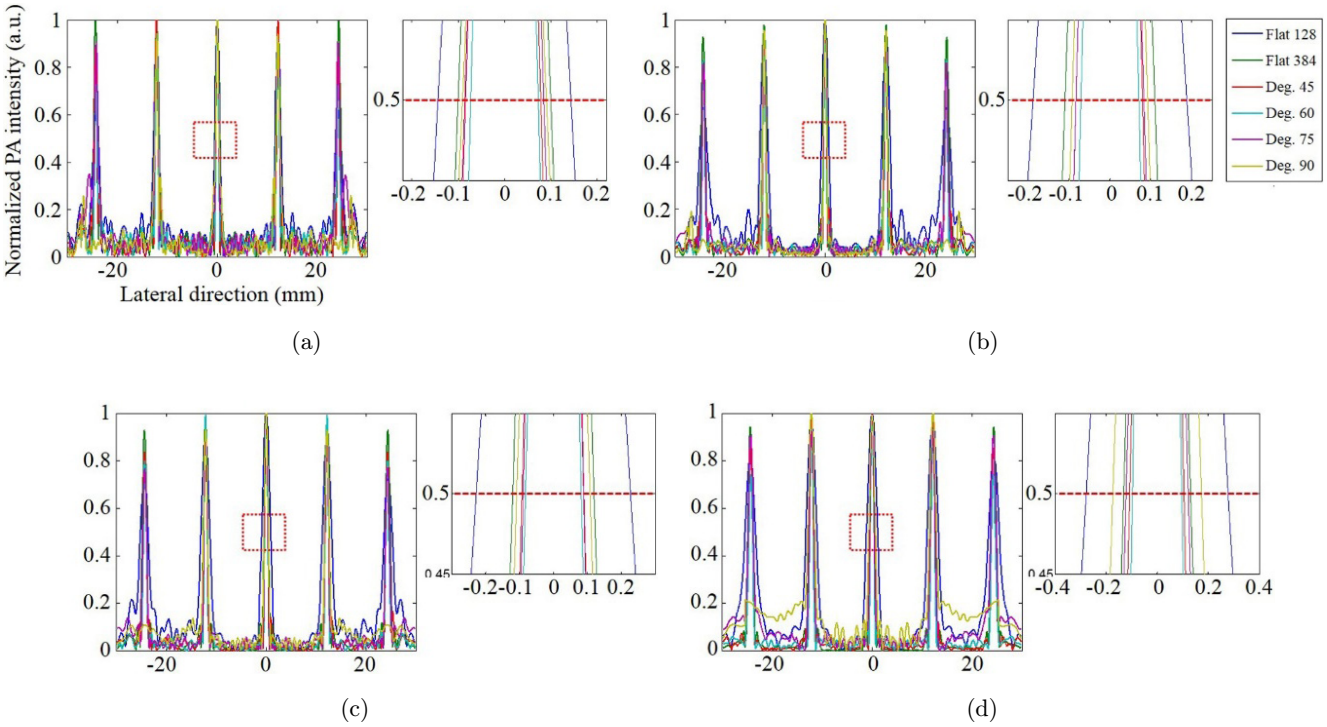

Fig. 6. (Color online) Quantitative analysis of enhanced resolution in synthetic aperture PAT. Lateral profiles of the normalized PA intensity along the point targets in the (a) second, (b) third, (c) fourth, and (d) fifth rows from the indicated aperture orientation. The box shown to the right of each plot is the zoom-in area corresponding to the dashed red box.

could provide quantitative verification of the aperture orientation effect on image resolution. The targets in the first row were ignored due to the fact that they were covered by the detectors in all the synthetic apertures. Comparing the full-width at half-maximum (FWHM) values of the targets in each row, the size of the center point target (true size of the point target is 0.10 mm) recovered from aperture orientation of 60° is entirely smaller than other aperture orientations, especially the single flat aperture case. For instance, the FWHM at the center point target [indicated by arrows in Figs. 5(a) and 5(d)] is calculated to be 0.20 ± 0.02 mm and 0.64 ± 0.08 mm for the synthetic aperture and the single aperture, respectively. Therefore, the aperture orientation of 60° in the synthetic aperture configuration is optimal to obtain the preferable image resolution with a relatively large detection FOV. The above quantitative results indicate that this aperture orientation can reconstruct the targets with higher resolution and imaging accuracy in the overall detection area, even the point targets located outside the blue shaded region but still in green shaded area can be recovered with an enhanced image resolution.

3.3. *Phantom study of the aperture orientation in the synthetic aperture PAT*

The phantom studies that could demonstrate the enhanced resolution and limited-view compensation problem were subsequently conducted. In the first step, due to the practicability of only one linear-array transducer, a small, point-like photoacoustic calibration target was rotated to calibrate the transducer position[34] in the synthetic aperture configuration. The synthetic aperture PAT was established with the same configuration as in simulation by rotating the imaging phantom with a fixed single linear-array transducer. A black human hair with a diameter of 80 μm was vertically placed at different rotating orientations of −60°, 0°, and 60° to calibrate the relative positions of the individual linear-array transducer. The corresponding rotation radius was 32.98 mm and the rotation center was located at the center of the overlapped detection region (the green shaded area in Fig. 1). The calibration process and results are shown in Fig. 7. Figures 7(a)–7(c) show the reconstructed PA images of −60°, 0°, and 60°, respectively. From the

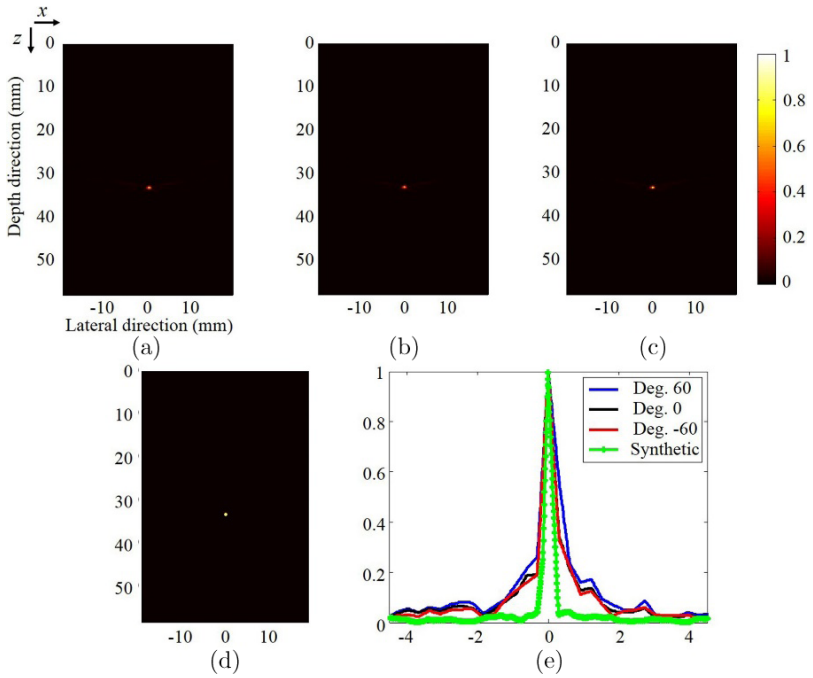

Fig. 7. Synthetic aperture PAT system calibration and enhanced resolution results. (a)–(c) PA images of the rotated phantom at the orientations of −60°, 0°, and 60°, respectively. (d) PA image reconstructed by the synthetic aperture. (e) Lateral profiles of the normalized PA intensity along the point target.

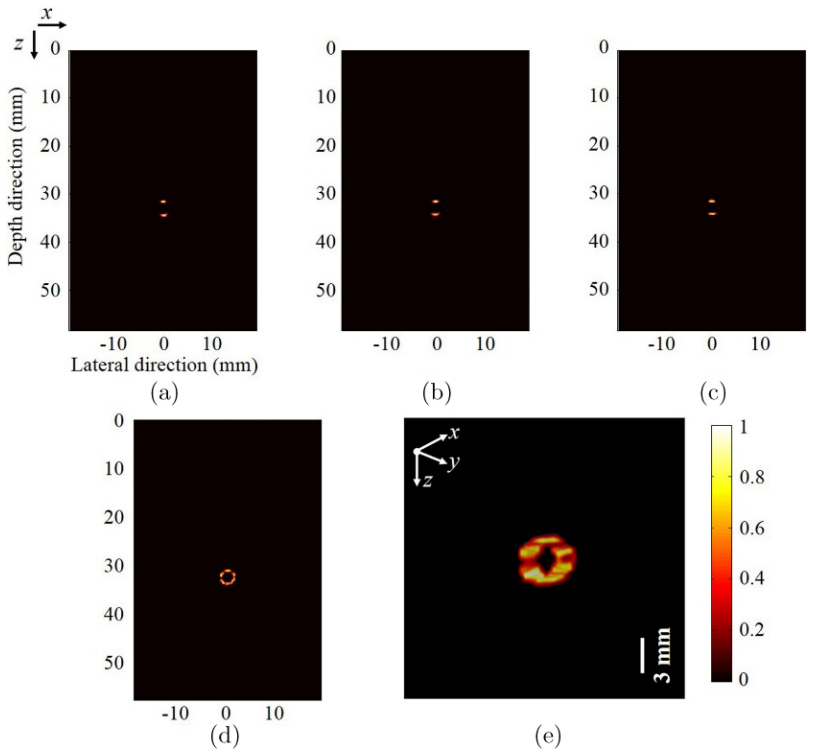

Fig. 8. Synthetic aperture PAT experiment results of limited-view compensation. (a)–(c) PA images of the rotated phantom at orientations of −60°, 0°, and 60°, respectively. (d) PA image reconstructed by the synthetic aperture in the cross-section. (e) Three-dimensional PA image of the target.

measurement of the depth and lateral position of this point target in PA images [see Figs. 7(a)–7(c)], the calibration target is practically located in the center of field of view. Thus the element positions in the synthetic aperture at an aperture orientation of 60° could be obtained for the offline PA image reconstruction.

Moreover, this calibration process also serves as the demonstration of enhanced resolution in this synthetic aperture PAT. Figure 7(d) shows the reconstructed PA image from the synthetic aperture at an aperture orientation of 60°, and Fig. 7(e) shows the corresponding quantitative analysis of this point target observed from the different single apertures and the synthetic aperture. The FWHMs for the synthetic aperture and the single aperture were calculated to be 0.25 ± 0.04 mm and 0.69 ± 0.11 mm, respectively, further demonstrating that the synthetic aperture could enhance the image resolution with reduced side lobe levels.

After the system calibration, a 3.0-mm-diameter polyethylene tube injected with India ink was designed as the imaging target to conduct the phantom study. The structure of the tube phantom could mimic the shape of blood vessel in real case. The light was distributed uniformly around the tube phantom. Figures 8(a)–8(c) respectively show the single aperture recovered results, i.e., for −60°, 0°, and 60°, where limited-view problem exists. The synthetic aperture restored results are shown in Figs. 8(d) and 8(e), respectively. Figure 8(d) is the two-dimensional cross-sectional PA image. Comparing Fig. 8(d) with the single aperture recovered results, it can be seen that this aperture orientation has the potential to overcome the limited-view challenge and thus it can provide nearly full-view imaging quality. The capability of the synthetic aperture PAT at this aperture orientation for three-dimensional PA imaging was also implemented based on the translational motion of the tube phantom, as shown in Fig. 8(e).

4. Discussion and Conclusion

As a consequence, the optimal field of view in the synthetic aperture PAT mainly determined by the aperture orientation effect can be verified and the corresponding optimal aperture orientation is 60°, considering the limited-view compensation and resolution enhancement. On the basis of conventional visible detection regions, this study further verified that the targets in the overlapped detection region could also minimize the limited-view problem with preferable resolution. Thus the optimal detection FOV in the synthetic aperture PAT includes the original visible detection region and the overlapped detection region from each single aperture, while the imaging quality in other regions is also improved. These simulation and phantom results matched well with the limited-view theory and the detection pattern of the linear-array transducer, i.e., only the boundaries of any objects inside the visible detection region can be recovered stably, while other sharp details may become blurred outside this region.

However, due to the limitation of hardware, only one linear-array ultrasound transducer was available in the phantom experiment. The synthetic aperture was formed by the relative rotation between the targets and transducer, rather than three individual linear-array transducers or a curved-array transducers. This work is thus a proof of concept study for the design of multi-segment curved-array transducer in our next study, which can compensate the limited-view artifact with enhanced resolution.

In summary, the aperture orientation effect in the synthetic aperture-based linear-array PAT was investigated. Through the placement of linear-array transducer at different aperture orientations, the optimal detection coverage providing full-view imaging quality and enhanced image resolution is achieved via the numerical simulation. The aperture orientation of 60° could successfully recover the originally invisible target structure and enhance the image resolution additionally. The optimal detection field of view in the synthetic aperture includes the original visible detection region and the overlapped detection region from each single aperture. Both the simulation and phantom results verified that the synthetic aperture could address the limited-view problem, and these results are well in agreement with the theory. This research could provide guidance for the fabrication of multi-segment curved-array transducer in our future study, which would be applied to the super-resolution whole-body photoacoustic tomography for small animals.

Conflict of Interest

The authors have no relevant financial interests in this article and no potential conflicts of interest to disclose.

Acknowledgments

This work is partially supported by the National Natural Science Foundation of China (Grant No. 61371045), Science and Technology Development Plan Project of Shandong Province, China (Grant No. 2016GGX103032), China Postdoctoral Science Foundation (Grant No. 2015M571413) and Shenzhen Science & Technology Program (No. JCYJ20160429115309834).

References

1. L. V. Wang, J. Yao, "A practical guide to photoacoustic tomography in the life sciences," *Nat. Methods* **13**, 627–638 (2016).
2. C. Lutzweiler, D. Razansky, "Optoacoustic imaging and tomography: Reconstruction approaches and outstanding challenges in image performance and quantification," *Sensors* **13**, 7345–7384 (2013).
3. B. Cox, J. G. Laufer, S. R. Arridge, P. C. Beard, "Quantitative spectroscopic photoacoustic imaging: A review," *J. Biomed. Opt.* **17**, 1660–1668 (2012).
4. L. V. Wang, "Multiscale photoacoustic microscopy and computed tomography," *Nat. Photonics* **3**, 503–509 (2009).
5. B. Y. Hsieh, S. L. Chen, T. Ling, L. J. Guo, P. C. Li, "All-optical scanhead for ultrasound and photoacoustic dual-modality imaging," *Opt. Express* **20**, 1588–1596 (2012).
6. L. Zhao, M. Yang, Y. Jiang, C. Li, "Optical fluence compensation for handheld photoacoustic probe: An *in vivo* human study case," *J. Innov. Opt. Health Sci.* **10**, 1740002-1–1740002-8 (2017).
7. Y. Wang, D. Xu, S. Yang, D. Xing, "Toward *in vivo* biopsy of melanoma based on photoacoustic and ultrasound dual imaging with an integrated detector," *Biomed. Opt. Express* **7**, 279–286 (2016).
8. X. Lin, M. Sun, N. Feng, D. Hu, Y. Shen, "Monte Carlo light transport-based blood vessel quantification using linear array photoacoustic tomography," *Chin. Opt. Lett.* **15**, 111701 (2017).
9. M. Xu, L. V. Wang, "Analytic explanation of spatial resolution related to bandwidth and detector aperture size in thermoacoustic or photoacoustic reconstruction," *Phys. Rev. E* **67**, 056605-1–056605-15 (2003).
10. Y. Xu, L. V. Wang, G. Ambartsoumian, P. Kuchment, "Reconstructions in limited-view thermoacoustic tomography," *Med. Phys.* **31**, 724–733 (2004).
11. H. Guo, W. Qi, M. He, J. Rong, L. Xi, "Co-registered photoacoustic and ultrasound imaging for tongue cancer detection," *J. Innov. Opt. Health Sci.* **11**, 1850008-1–1850008-8 (2017).
12. B. Huang, J. Xia, K. Maslov, L. V. Wang, "Improving limited-view photoacoustic tomography with an acoustic reflector," *J. Biomed. Opt.* **18**, 655–661 (2013).
13. G. Li, J. Xia, K. Wang, K. Maslov, M. A. Anastasio, L. V. Wang, "Tripling the detection view of high-frequency linear-array-based photoacoustic computed tomography by using two planar acoustic reflectors," *Quant. Imaging Med. Surg.* **5**, 57–62 (2014).
14. R. Ellwood, E. Zhang, P. Beard, B. Cox, "Photoacoustic imaging using acoustic reflectors to enhance planar arrays," *J. Biomed. Opt.* **19**, 126012 (2014).
15. B. T. Cox, S. R. Arridge, P. C. Beard, "Photoacoustic tomography with a limited-aperture planar sensor and a reverberant cavity," *Inverse Probl.* **23**, S95 (2007).
16. R. A. Kruger, K. W. Kiser, Jr., D. R. Reinecke, G. A. Kruger, "Thermoacoustic computed tomography using a conventional linear transducer array," *Med. Phys.* **30**, 856–860 (2003).
17. D. Yang, D. Xing, S. Yang, L. Xiang, "Fast full-view photoacoustic imaging by combined scanning with a linear transducer array," *Opt. Express* **12**, 15566–15575 (2007).
18. X. Lin, N. Feng, Y. Qu, D. Chen, Y. Shen, M. Sun, "Compressed sensing in synthetic aperture photoacoustic tomography based on a linear-array ultrasound transducer," *Chin. Opt. Lett.* **15**, 101102 (2017).
19. M. Cao, J. Yuan, S. Du, G. Xu, X. Wang, P. L. Carson, X. Liu, "Full-view photoacoustic tomography using asymmetric distributed sensors optimized with compressed sensing method," *Biomed. Signal Process. Control* **21**, 19–25 (2015).
20. M. Xu, L. V. Wang, "Pulsed-microwave-induced thermoacoustic tomography: Filtered backprojection in a circular measurement configuration," *Med. Phys.* **29**, 1661–1669 (2002).
21. M. Xu, L. V. Wang, "Universal back-projection algorithm for photoacoustic computed tomography," *Phys. Rev. E* **71**, 016706-1–016706-7 (2005).
22. X. Liu, D. Peng, X. Ma, W. Guo, Z. Liu, D. Han, X. Yang, J. Tian, "Limited-view photoacoustic imaging based on an iterative adaptive weighted filtered backprojection approach," *Appl. Opt.* **52**, 3477–3483 (2013).

23. D. Yang, D. Xing, H. Gu, Y. Tan, L. Zeng, "Fast multielement phase-controlled photoacoustic imaging based on limited-field-filtered back-projection algorithm," *Appl. Phys. Lett.* **87**, 194101 (2005).
24. M. M. Nguyen, X. Ding, S. A. Leers, K. Kim, "Multi-focus beamforming for thermal strain imaging using a single ultrasound linear array transducer," *Ultrasound Med. Biol.* **43**, 1263–1274 (2017).
25. M. Mozaffarzadeh, A. Mahloojifar, M. Orooji, S. Adabi, M. Nasiriavanaki, "Double stage delay multiply and sum beamforming algorithm: Application to linear-array photoacoustic imaging," *IEEE Trans. Biomed. Eng.* **65**, 31–42 (2018).
26. M. Oeri, W. Bost, M. Fournelle, "Analytical calibration of linear transducer arrays for photoacoustic tomography," *Proc. SPIE* **9539**, 95390P (2015).
27. J. Xia, J. Yao, L. V. Wang, "Photoacoustic tomography: Principles and advances," *Electromagn. Waves (Camb.)* **147**, 1–22 (2014).
28. D. Cai, Z. Li, S.-L. Chen, "Photoacoustic microscopy by scanning mirror-based synthetic aperture focusing technique," *Chin. Opt. Lett.* **13**, 101101 (2015).
29. C. Li, L. V. Wang, "High-numerical-aperture-based virtual point detectors for photoacoustic tomography," *Appl. Phys. Lett.* **93**, 33902 (2008).
30. H. K. Zhang, E. Ergun, G. E. Trahey, E. M. Boctor, "Synthetic aperture ultrasound imaging with robotic aperture extension," *Proc. SPIE* **9419**, 94190L (2015).
31. J. Gateau, M. A. Caballero, A. Dima, V. Ntziachristos, "Three-dimensional optoacoustic tomography using a conventional ultrasound linear detector array: Whole-body tomographic system for small animals," *Med. Phys.* **40**, 013302 (2013).
32. G. Li, L. Li, L. Zhu, J. Xia, L. V. Wang, "Multiview Hilbert transformation for full-view photoacoustic computed tomography using a linear array," *J. Biomed. Opt.* **20**, 066010 (2015).
33. B. E. Treeby, B. T. Cox, "k-Wave: MATLAB toolbox for the simulation and reconstruction of photoacoustic wave fields," *J. Biomed. Opt.* **15**, 021314 (2010).
34. J. J. L. Carson, P. Ephrat, A. Seabrook, "Measurement of photoacoustic transducer position by robotic source placement and nonlinear parameter estimation," *Proc. SPIE* **6856**, 68561Z (2008).